Collinear acousto-optical filters controlled by acoustic waves of finite amplitude

Technical Report No. 616

Principal contributors:

Alexandre S. Shcherbakov[(1)], Adán Omar Arellanes[(1)], Emanuele Bertone[(1)], and **Sergey A. Nemov[(2)].**

[(1)]National Institute for Astrophysics, Optics, and Electronics (INAOE), Puebla, Mexico.

[(2)]Saint – Petersburg State Polytechnic University, Polytechnicheskaya Str. 29, St-Petersburg, 195251, Russian Federation

National Institute for Astrophysics, Optics, and Electronics (INAOE),

Puebla, Mexico.

Department for Optics, INAOE

INAOE, 2015
The authors hereby grant to INAOE permission to reproduce and distribute copies of this technical report.

Index

1. Introduction 3

2. A three-wave collinear interaction with the phase mismatches and linear acoustic losses 5

3. Applying the conditions of extrema efficiencies to light scattering 7

4. Transmission function for collinear acousto-optical interaction 10

4.1. Factors affecting the spectral resolution of electronically tunable acousto-optical filters 11

4.1.1. Light-induced absorption and photorefraction in $LiNbO_3$ crystals 13

4.1.2. Nonlinear absorption 13

5. Scheme for the experiments with a collinear acousto-optical cells 19

6. Experiments with collinear acousto-optical filters 20

6.1 Calcium molybdate cell 20

6.1.1. Lossless case 20

6.1.2. Lossy case ..22

6.2 Lithium niobate cell 25

7. Conclusion 29

8. Acknowledgments 29

9. References 29

ABSTRACT

New physical aspects of collinear acousto-optical interaction, occurred by acoustic waves of finite amplitude, are revealed and analyzed in crystalline materials exhibiting moderate linear acoustic losses. The analysis is performed in the regime of continuous traveling waves allowing specific mechanism of the acousto-optic nonlinearity. Our consideration has shown that such nonlinearity together with linear acoustic losses is able to affect the transmission function inherent in collinear interaction. In particular, the mere presence of linear acoustic losses by themselves leads to broadening the width of transmission function beginning already from very low levels of the applied acoustic power. Moreover, the transmission function exhibits a marked and quasi-periodical dependence on the applied acoustic power density; and that periodicity is governed by the linear acoustic losses. As a result, the transmission function can be significantly narrowed near isolated points at the cost of decreasing the interaction efficiency. These novelties related to collinear acousto-optical interaction accompanied by moderate linear acoustic losses have been studied and confirmed experimentally with two advanced acousto-optical cells based on calcium molybdate ($CaMoO_4$) single crystal and lithium niobate ($LiNbO_3$), which are controlled by acoustic waves of finite amplitude. For the lithium niobate cell we examine the phenomena affecting the filter transmission efficiency and its spectral resolution, namely, the light-induced absorption and photorefraction. The highest available spectral resolution attains $\delta\lambda = 0.15$ Å at $\lambda = 370$ nm (the resolving power $R \sim 25000$), with an efficiency of 11%, or $\delta\lambda = 0.18$ Å at $\lambda = 532$ nm ($R \sim 30000$), with an efficiency of 33%.

Key words: Dynamic gratings, Acousto-optical filter, Parametric processes, High spectral resolution, Acousto-optical devices

1. INTRODUCTION

Collinear acousto-optical interaction had been initially revealed in the middle of the sixties past century by R.W. Dixon [1] and then, starting from the seventies has been successfully studied and exploited in various applications, among which first of all one has to call the tunable acousto-optical filters [2–6]. The conventional analysis of this phenomenon in terms of lossless plane waves was presented in a number of classical issues [7,8]. It allows the application of a given acoustic field approximation or, what is the same, the regime of a weak coupling, when the spatial distribution of acoustic beam along a crystalline material is almost independent on the spatial distribution of light that leads to considerable theoretical and practical simplifications. In particular, a 100% efficiency of light scattering may be achieved without any effect on the acoustic beam in this case, so the above-mentioned control can be repeated for a lot of times with almost no losses of acoustic energy. Moreover, an essential difference between velocities of light and ultrasound gives us an opportunity for applying the quasi-stationary approximation to the analysis of modern problems related to collinear interaction. In the past decades great progress has been made in acousto-optics and now it is a widely used technique in the field of data processing [9,10]. Nevertheless, recently the existence of a new branch in studies and applications of collinear acousto-optical interaction, which is associated with acousto-optical nonlinearity, for example, in the form of three-wave coupled states, has been manifested [11-13]. That is why we believe that it is a worthwhile investment to develop these investigations, because the objects being under consideration here are closely connected with the above-mentioned nonlinearity in the regime of a weak coupling. Within this consideration, we develop the exact and closed analytical model of the collinear light scattering by continuous

traveling acoustic waves of finite amplitude in a birefringent material with moderate linear acoustic losses. The main attention is paid to the distribution of the scattered light intensity, which can be considered as the transmission function of this process in the context of our analysis. In its turn, the width of the transmission function can be directly associated with the frequency resolution of the equivalent collinear acousto-optical filter. In so doing, we analyze the peculiarities of the effect conditioned by the acousto-optical nonlinearity, which leads to a measurable dependence of the transmission function on both the applied power density of acoustic waves of finite amplitude and the linear acoustic losses in crystalline material

Theoretically assumed novel properties of the collinear acousto-optical interaction accompanied by nonlinearity and moderate linear acoustic losses are investigated experimentally with an advanced acousto-optical cell made of calcium molybdate ($CaMoO_4$) and lithium niobate ($LiNbO_3$) crystal and controlled by acoustic waves of finite amplitude.

2. A THREE-WAVE COLLINEAR INTERACTION WITH THE PHASE MISMATCHES AND LINEAR ACOUSTIC LOSSES

A three-wave co-directional collinear interaction with the mismatched wave numbers in a two-mode medium is described by a set of three nonlinear partial differential equations [11]. Here, we consider the regime of a weak coupling [12,13], when two light modes are scattered by relatively slow wave, being non-optical by its nature and exhibiting the linear losses, when essentially effective Bragg scattering of light can be achieved without any observable influence of the scattering process on that non-optical wave, because the number of interacting photons is a few orders less than the number of the scattering quanta injected into a medium. Then, the velocities of light modes can be approximated by the same value c, because usually the length of crystalline materials does not exceed $20\,cm$. In this regime, the above-mentioned set of equations falls into an equation for the complex amplitude $U(x,t)$ of a slow wave (V is the velocity of this wave) and a pair of the combined equations for the complex amplitudes $C_0(x,t)$ and $C_1(x,t)$ of the incident (pumping) light wave and scattered one, respectively,

$$\text{a)}\quad \frac{\partial U}{\partial x}+\frac{1}{V}\frac{\partial U}{\partial t}=-\alpha U\,,$$

$$\text{b)}\quad \frac{\partial C_0}{\partial x}+\frac{1}{c}\frac{\partial C_0}{\partial t}=-q_1\,C_1U^*\exp\,(2i\eta\,x)\,,$$

$$\text{c)}\quad \frac{\partial C_1}{\partial x}+\frac{1}{c}\frac{\partial C_1}{\partial t}=q_0\,C_0U\exp\,(-2i\eta\,x)\,. \qquad (1)$$

Here, the factor α describes the linear losses of non-optical wave, $q_{0,1}$ are the constants of interaction, and 2η is the mismatch of wave numbers inherent in the interacting waves. Now, we go to the tracking coordinates $(x,\tau=t-x/c)$ and assume that non-optical wave, governed by Eq.(1a) and described by $U=u[x(1-V/c)-V\tau]\exp(-\alpha x)\exp(i\varphi)$, has the constant phase φ. Then, we follow the analysis developed in Ref.[13] and study the quasi-stationary continuous-wave regime for both the incident light and the non-optical wave when $u[x(1-V/c)-V\tau]=U_0$ is constant. Equations (1) are analyzed with the fixed magnitude of the mismatch η and practically natural boundary conditions $a_0(x=0,t)=1$, $(\partial a_0/\partial x)(x=0,t)=0$, $a_1(x=0,t)=0$, and $(\partial a_1/\partial x)(x=0,t)=q_0U_0$ in a half-infinite medium. To construct the solution, which is valid for significant phase mismatches, i.e. when $\eta>\alpha$, we use the conservation law $q_0\,a_0^2+q_1\,a_1^2=q_0-\text{const}$, resulting from Eqs.(1). Due to the expected smallness of the factor α, one can suggest that the spatial scale of varying the term $\exp(\alpha x)$ is much larger than the scale of varying the derivative $\partial a_{0,1}^2/\partial x$. With the parameter $q_0q_1U_0^2=\sigma^2$, characterizing contributions of both the material properties and the acoustic power density, one can find [13] the stationary intensities of the pumping and scattered light waves

$$\text{(a)}\ \ |C_0(x)|^2 = \frac{\eta^2}{\sigma^2+\eta^2} + \frac{\sigma^2}{\sigma^2+\eta^2}\ \cos^2\left[G(x)-G(0)\right],$$

$$\text{(b)}\ \ |C_1(x)|^2 = \frac{q_0}{q_1}\frac{\sigma^2}{\sigma^2+\eta^2}\ \sin^2\left[G(x)-G(0)\right]. \qquad (2)$$

$$G(x) = \frac{1}{\alpha}\left[-\sqrt{\eta^2+\sigma^2\exp(-2\alpha x)} + \eta\ \ln\left\{\frac{2\alpha}{\eta^2}\left[\eta\ \exp(\alpha x)+\sqrt{\sigma^2+\eta^2\exp(2\alpha x)}\ \right]\right\}\right]. \qquad (3)$$

These solutions include contributions of two types. The first summand in the intensity $|C_0|^2$ represents a background determined by the mismatch η; the second one gives the oscillations imposed on that background. The scattered light wave contains only oscillations without a background.

3. APPLYING THE CONDITIONS OF EXTREMA EFFICIENCIES TO LIGHT SCATTERING

Obviously, each extrema can be reached at $\eta = 0$, so that the position of extrema is conditioned by the losses α and the parameter σ. When $\eta = 0$, one yields $G(x) = -\alpha^{-1}\sigma \exp(-\alpha x)$, so that Eq.(2b) takes the form

$$\left| C_1(x) \right|^2 = \frac{q_0}{q_1} \sin^2 \left\{ \frac{\sigma}{\alpha} \left[1 - \exp(-\alpha x) \right] \right\} . \tag{4}$$

Now, one can involve conditions of reaching maxima and zeros in the scattered light distribution as

$$\text{a) Maxima:} \quad G(x) - G(0) = \pi \left(N + \frac{1}{2} \right), \; N = 0,1,2, \ldots ;$$

$$\text{b) Zeros:} \quad G(x) - G(0) = \pi \, M , \qquad M = 1,2,3, \ldots , \tag{5}$$

where N and M are the numbers of maxima and zeros, respectively. .These conditions lead to the equalities

$$\text{a)} \quad \frac{\sigma}{\alpha} \left[1 - \exp(-\alpha x) \right] = \pi \left(N + \frac{1}{2} \right) ,$$

$$\text{b)} \quad \frac{\sigma}{\alpha} \left[1 - \exp(-\alpha x) \right] = \pi \, M . \tag{6}$$

Because the left hand sides of these formulas are limited, one can find that

$$\text{a)} \quad N \le \frac{\sigma}{\alpha \pi} \left[1 - \exp(-\alpha x) \right] - \frac{1}{2} ,$$

$$\text{b)} \quad M \le \frac{\sigma}{\alpha \pi} \left[1 - \exp(-\alpha x) \right] , \tag{7}$$

i.e. the numbers N and M are restricted. Moreover, it is seen that $N \le \frac{\sigma}{\alpha \pi} - \frac{1}{2}$ and $M \le \frac{\sigma}{\alpha \pi}$ with $x \to \infty$.

At first, let us consider the maxima. Equation (4) can be illustrated by the following $2D$ contour-plot, which represents a few cross-sections of the right hand side of Eq.(7a) by planes $N = 0,1,2$, see Fig.1. The unit-valued maxima of Eq.(4) under condition imposed by Eq.(5a) are placed at the distances

$$X_N = -\alpha^{-1} \cdot \ln \left[1 - \frac{\alpha \pi}{\sigma} \left(N + \frac{1}{2} \right) \right] . \tag{8}$$

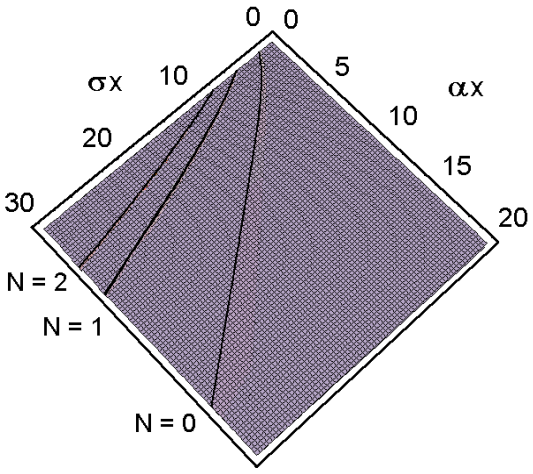

Fig.1. A 2D contour-plot on the plane [αx , σx] with lines corresponding to $N = 0, 1, 2$

For example, (1) when $\alpha = 0.1\, cm^{-1}$ and $\sigma = 0.5\, cm^{-1}$, one arrives at $N \le 1$ with $X_0 = 3.768\, cm$ and $X_1 = 28.55\, cm$; (2) when $\alpha = 0.1\, cm^{-1}$ and $\sigma = 1\, cm^{-1}$, one yields $N \le 2$, wherein $X_0 = 1.709\, cm$, $X_1 = 6.372\, cm$, and $X_2 = 15.39\, cm$, see Fig.2; (3) while when $\alpha = 0.1\, cm^{-1}$ and $\sigma = 2\, cm^{-1}$, one has $N \le 5$ with $X_0 = 0.818\, cm$, $X_1 = 2.687\, cm$, $X_2 = 4.987\, cm$, $X_3 = 7.980\, cm$, $X_4 = 12.271\, cm$, and $X_5 = 19.964\, cm$. Together with this in the medium with much lower acoustical losses, let say for instance with $\alpha = 0.01\, cm^{-1}$, one can find $N \le 15$ for $\sigma = 0.5\, cm^{-1}$. Together with this, Eq.(6) gives another illustration for positions of the unit-valued maxima. The corresponding plot for $N = 0$ is given by Fig.3.

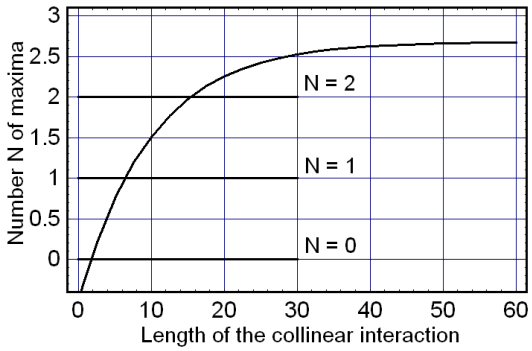

Fig.2. Restricting the number N of unit-valued maxima in the case $\alpha = 0.1\, cm^{-1}$ and $\sigma = 1\, cm^{-1}$

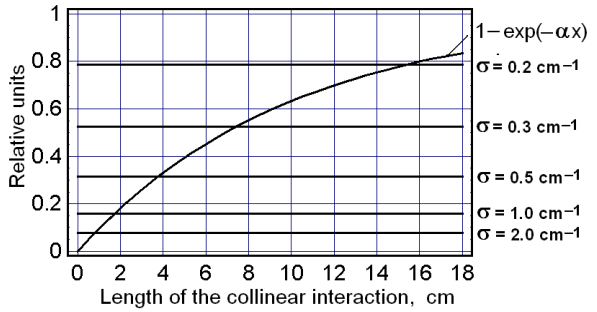

Fig.3. Positions for the unit-valued maxima as functions of the collinear interaction length and σ as a parameter.

At this step, one can analyze the zeros in the light intensity $|C_1|^2$ distribution. In so doing, Eq.(4) can be illustrated by a $2D$ contour-plot, which represents a few cross-sections of the right hand side of Eq.(7b) by planes $M = 1, 2, 3, \ldots$, which is quite similar to Fig.1. The zero-intensity points are placed at the distances

$$Z_M = -\alpha^{-1} \cdot \ln\left[1 - \frac{\alpha\pi}{\sigma} M\right]. \tag{9}$$

For example, (1) when $\alpha = 0.1\,cm^{-1}$ and $\sigma = 0.5\,cm^{-1}$, one arrives at $0 < M \le 1$ with $Z_1 = 9.89\,cm$; (2) when $\alpha = 0.1\,cm^{-1}$ and $\sigma = 1\,cm^{-1}$, one yields $0 < M \le 3$, wherein $Z_1 = 3.77\,cm$, $Z_2 = 9.89\,cm$, and $Z_3 = 28.47\,cm$, see Fig.4; (3) while when $\alpha = 0.1\,cm^{-1}$ and $\sigma = 2\,cm^{-1}$, one has $0 < M \le 6$ with $Z_1 = 1.708\,cm$, $Z_2 = 3.77\,cm$, $Z_3 = 6.386\,cm$, $Z_4 = 9.89\,cm$, $Z_5 = 15.37\,cm$, and $Z_6 = 28.47\,cm$.

Finally, Eq.(4) can be directly exploited for illustrating the light intensity dependences under consideration. In the above-noted approximation $q_0 / q_1 \approx 1$ one can obtain the plots presented in Fig.4. The extrema of each individual curve are coincided with the calculated above values for X_N and Z_M, see Eqs.(8) and (9). At this step of analysis, one has to remind about the above-exploited approximation within solving Eq.(5) and to note that Eqs.(6) as well as their solutions in the forms of Eqs.(8) and (2) are not valid for infinite distances

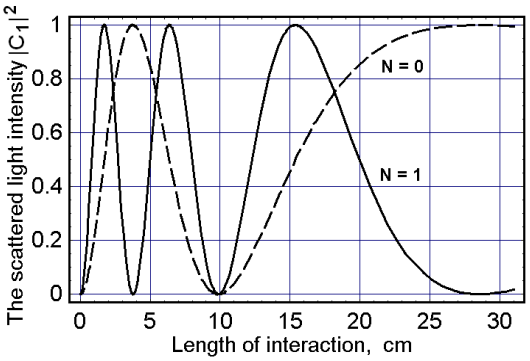

Fig.4. The normalized scattered light distributions versus the dimensional length of interaction with $\alpha = 0.1\,cm^{-1}$: the dashed line is for $\sigma = 0.5\,cm^{-1}$ and solid line is for $\sigma = 1\,cm^{-1}$

4. TRANSMISSION FUNCTION FOR COLLINEAR ACOUSTO-OPTICAL INTERACTION

It is well known [2-6] that the transmission function width (TFW) δf of the collinear acousto-optical interaction is usually estimated by $\delta f = V/L$, where V is the acoustic wave velocity and L is the longitudinal aperture of crystal, i.e. the length of acousto-optical interaction. It is obviously seen that the this formula does not include both the acoustic attenuation and the potential influence of initial acoustic power density on the TFW.

At first, let us consider Eqs.(4) and (6b) in the lossless medium with $\alpha = 0$ and in the case of infinitely small signals, i.e. with $\sigma \to 0$. In so doing, one can estimate $G(x, \alpha = 0) = \eta x$, $G(0, \alpha = 0) = 0$, and write

$$\left| C_1(x) \right|^2 = \left(\frac{q_0 \, (\sigma x)^2}{q_1} \right) \cdot \frac{\sin^2 (\eta x)}{(\eta x)^2} \ , \tag{10}$$

where the distance x can be considered as a parameter. Historically, estimating the TFW is connected with the well-known Rayleigh criterion, which predicts in fact separating a pair of the neighboring $(\sin u/u)^2$ – shaped distributions at the intensity level of $\nu \approx 0.4055$. This is exactly the case of Eq.(10), and one has to resolve the transcendent algebraic equation $\sin (\eta x) = \nu^{1/2} (\eta x) \approx 0.6368 \, (\eta x)$. The first (both positive and negative) solutions to this algebraic equations are $\eta_{(\pm)} x = \pm \pi/2$. They lead to the bandwidth from $\eta_{(-)} x = -\pi/2$ to $\eta_{(+)} x = +\pi/2$, i.e. to the full bandwidth at the intensity level: $\nu \approx 0.4055$, which is given by $\Delta \eta x = \eta_{(-)} x + \eta_{(+)} x = |-\pi/2| + |+\pi/2| = \pi$. Together with this a one-side mismatch η had been previously [see Eqs.(1)] determined as $\eta = \Delta K/2 = \pi \delta f / V$, so that in the more detailed form $\eta_{(\pm)} = \pi \delta f_{(\pm)} / V$ (where $\delta f_{(\pm)}$ are the corresponding one-side frequency deviations) and consequently, the total deviation of the mismatch is given by $\Delta \eta = \eta_{(-)} + \eta_{(+)} = \pi (\delta f_{(-)} + \delta f_{(+)}) / V = \pi \delta f / V$. Combining the expressions, which include $\Delta \eta$, one arrives at the above-noted formula $\delta f = V/x$, where one can undoubtedly put $x = L$. Thus, one can see that full width of the main lobe inherent in the $(\sin u/u)^2$ – distribution at the intensity level $\nu \approx 0.4055$ gives the "standard" determination of the frequency resolution in acousto-optics or the TFW, which is conditioned by the limit $\sigma \to 0$. In the case of a moderately lossy medium, i.e. with $\alpha \neq 0$ and $\sigma \to 0$, Eqs.(3) give us

$$\text{a)} \ G(x, \alpha \neq 0) = \alpha^{-1} \eta \, [\alpha x - 1 + \ln (4 \alpha \eta^{-1})],$$

$$\text{b)} \ G(0, \alpha \neq 0) = \alpha^{-1} \eta \, [-1 + \ln (4 \alpha \eta^{-1})] \ . \tag{11}$$

As a result, $G(x, \alpha \neq 0) - G(0, \alpha \neq 0) = \eta x$ as well and one arrives at Eq.(10). Consequently, the traditional conclusion lies in the fact that under condition of infinitely small signals, i.e. with $\sigma \to 0$, the acoustic losses do not affect the TFW independently on the concrete level of those linear losses.

Then, one can naturally consider Eq.(10) in the case of $\alpha \neq 0$ under acting the signals of finite amplitude when $\sigma \neq 0$. The 3D-plots peculiar to these distributions are presented in Fig.5 for the scattered light intensity $\left|C_1(x)\right|^2$ in terms of the absolute units in practically reasonable approximation $q_0 / q_1 \approx 1$ on the interval $0 \le \sigma x \cong 3\pi$. Regular structures exhibit reaching a sequence of unit-valued maxima along the line $\eta x = 0$ within various dimensionless $\sigma x-$periods depending on the product $\alpha x \neq 0$. In fact, one can consider the result of growing the product αx as a scaling along the $\sigma x-$axis, which leads to a shift of unit-valued maxima in the larger $\sigma x-$direction.

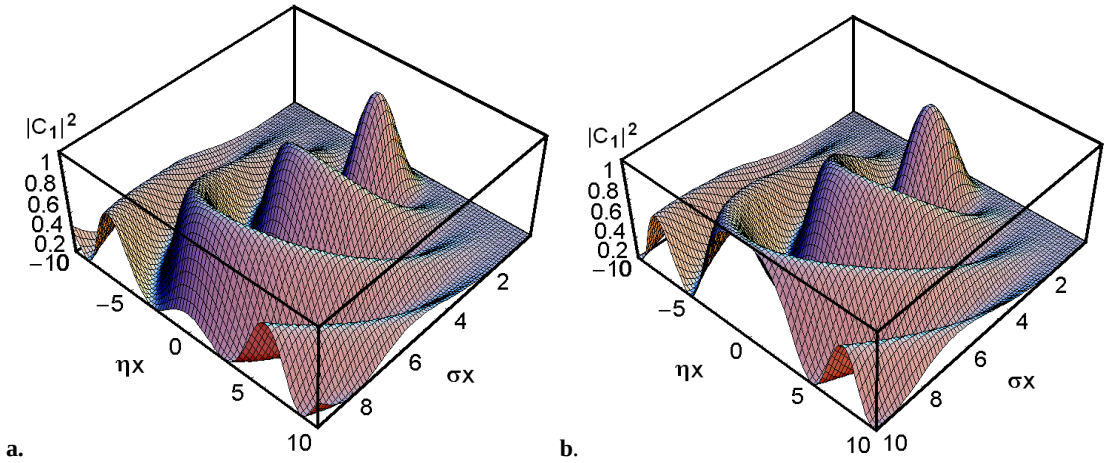

Fig.5. The 3D plots for the absolute values of the scattered light intensity profile with $\alpha \neq 0$ and $q_0 / q_1 \approx 1$ on the interval $0 \le \sigma x \cong 3\pi$: (**a**) $\alpha x = 0.1$ and (**b**). $\alpha x = 0.5$.

In the case of a moderate acoustical losses, Eqs.(2) and (3) should be exploited in their original forms as well with $\alpha \neq 0$ and $\sigma \neq 0$. The above-formulated requirement of maximal efficiency of light scattering leads to Eqs.(5) and (6) as well as to Figs.1,2.

4.1. Factors affecting the spectral resolution of electronically tunable acousto-optical filters

Realizing the collinear acousto-optical interaction between ideally plane light and acoustic waves is associated with the following conservation law $k_0 + K = k_1$ for the wave numbers of the interacting waves. It can be rewritten as $n_0 / \lambda + f / V = n_1 / \lambda$, where $k_{0,1}$ are the wave numbers of the incident and scattered light waves, respectively; $n_{0,1}$ are the corresponding refractive indices; λ is the wavelength of the incident light; while f and V are the carrier frequency and the velocity of the acoustic wave with the wave number K. The last equation determines the acoustic carrier frequency as

$$f = \frac{|n_1 - n_0|V}{\lambda} \ . \qquad (12)$$

This set of considerations is mainly focused on the blue-visible and near ultraviolet range of the optical spectrum, so that initially one can estimate the parameters in the AOF for the visible wavelength $\lambda = 405\,nm$.

Widely used acousto-optical filters operate in the traveling-wave regime at relatively low radio-frequency acoustic waves and exploit such materials as $\alpha-$quartz ($\alpha-SiO_2$) or calcium molybdate ($CaMoO_4$) single crystals. Nevertheless, in the acoustically and optically lossless approximations and under action of the acoustic wave of "infinitely small amplitude", the spectral resolution $\delta\lambda_0$ of similar filters is usually estimated by the formula

$$\delta\lambda_0 = \lambda^2/(|\Delta n|L)\ , \tag{13}$$

which does not include any parameters of acoustic wave and, besides the length of interaction L, depends only on the birefringence $|\Delta n| = |n_1 - n_0|$ peculiar to a crystal and the light wavelength λ.

After the introductive consideration of traditional approach to the spectral resolution $\delta\lambda_0$ in the frames of Eq.(13), one has to touch the other phenomena that can potentially affect the spectral resolution, specially in the $LiNbO_3$-crystal based AOF, due to variations of birefringence. In doing so, the refined spectral resolution $\delta\lambda_R$ can be formally represented as a sum of variations of the inverted Eq.(12) in the first approximation

$$\delta\lambda_R = \frac{\lambda}{|\Delta n|}\left[-\frac{|\Delta n|}{f}\delta f + \left(\frac{\partial|\Delta n|}{\partial\lambda}\right)\delta\lambda + \Delta B + \left(\frac{\partial|\Delta n|}{\partial T}\right)\delta T + \left(\frac{\partial|\Delta n|}{\partial I}\right)\delta I\right] \tag{14}$$

with the above-noted conservation law $V/f = \lambda/|\Delta n|$. Here, ΔB is the non-uniformity of the birefringence, δT is the change in temperature of the operating acousto-optical cell, and δI is the change of the light intensity along the crystal. The first term in Eq.(14) leads to Eq.(13) and gives the traditional expression for the spectral resolution. The second term characterizes the dispersion of birefringence in a crystal, which can be combined from point to point with contribution of the first term as it had been mentioned above within the comments to Eq.(13).

Consequently, the combined contribution of two first terms in Eq.(14) can be expressed as

$$\delta\lambda_0 \approx -\frac{\lambda^2}{|\Delta n|L}\left[1 + \frac{\lambda}{|\Delta n|}\left(\frac{\partial|\Delta n|}{\partial\lambda}\right)\right], \tag{15}$$

where the traditional formulas $\delta f \approx V/L$ and $\delta\lambda = -\lambda^2/(|\Delta n|L)$ for the corresponding variations in Eq.(14) had been used in the zero approximation.

Then, the third term in Eq.(14) reflects optical non-uniformity of the birefringence in a crystal, i.e. variation of the birefringence $|\Delta n|$ due to optical imperfectness along a crystal. Because Eq.(14) includes the ratio $\lambda/|\Delta n| \sim 10^3\ Å$, while the desirable spectral resolution had been estimated at least

by $\delta\lambda_0 \le 0.1\,\text{Å}$, one should require $\Delta B \le 10^{-6}$ to get an opportunity for neglecting this summand in Eq.(14). Similar level of uniformity is acceptable within real practice.

The fourth term is the change in the birefringence due to changes in the temperature of the acousto-optical cell. These changes have been previously measured in lithium niobate to be about $\partial\,\Delta n/\partial T \approx 0.7216\times10^{-4}/°K$ [14]. At the same time, the existing technology allows stabilizing the temperature of AOCs to better than 0.002 °K [15]. Combining these two factors, one can estimate a change in the birefringence in the order of $\delta|\Delta n| \approx 10^{-7}$, which is small enough to be neglected from the analysis.

Finally, the last term in the right hand side describes the nonlinear behavior of the birefringence due to its potential dependence on the spatial distribution of an external light along a crystal. This effect is connected with varying the photorefraction, i.e. with its non-uniformity, so that the last term will be estimated in the next subsection.

4.1.1. Light-induced absorption and photorefraction in $LiNbO_3$ crystals

Exploiting $LiNbO_3$ crystal as a material for an AOF requires a set of additional estimations conditioned by the presence of the light-induced absorption and photorefraction in this material. These effects had been observed in $LiNbO_3$ crystals within the optical range from near ultraviolet to infrared radiation, and it might bring difficulties for optical spectroscopy due to reducing performances of an AOF. Nevertheless, the possibility exists to exploit this crystalline material, because its optical properties can be modified by relatively small concentrations of some dopants. There are a few dopants such as iron, magnesium or hafnium, which are widely investigated and used in various applications. Here, however, we will restrict ourselves only to Mg doped $LiNbO_3$ crystals [16,17] keeping in mind potential exploitation of an AOF in near ultraviolet range [18].

4.1.2. Nonlinear absorption

Originally, light absorption in Mg doped $LiNbO_3$ crystals can be characterized by the absorption factor $\alpha_0(\lambda)$ at an infinitely small incident optical power density. This factor is rather dispersive in behavior specifically near the edge of absorption, i.e. in near ultraviolet range, and it depends on the particular concentration of dopant. The first set of solid lines in Fig. 6a illustrates the behavior of the absorption factor $\alpha_0(\lambda)$ for the congruent $LiNbO_3$ crystal (CLN) and the congruent $LiNbO_3$ crystals doped by 4, 7 or 9 % of Mg (see notations Mg4, Mg7, and Mg9, respectively) under action of an infinitesimal incident optical power density. The second set of curves is presented for the near ultraviolet range in Fig. 6b. It shows the above-noted solid lines (conditioned by the absorption factor $\alpha_0(\lambda)$ only) together with the dotted lines, which depict the combined optical losses, including the light-induced absorption, governed by an additional external spectral flux I. This additional flux is chosen in such a way that contributions of the light-induced absorption do not exceed about 10% of the original optical losses $\alpha_0(\lambda)$ for all the considered concentrations of magnesium dopant [19]. Moreover, the additional flux has spectrally uniform distribution along all the visible and near ultraviolet ranges. Experimental data show [19] that the noted 10% excess over $\alpha_0(\lambda)$ means physically achieving the saturation of the light-induced absorption. After that, one can

find from Fig. 6 that the best option, i.e. appearing a minimal light-induced absorption, is associated evidently with 4% Mg doped $LiNbO_3$ crystal providing, for example, $\alpha_0(\lambda) \approx 0.28\, cm^{-1}$ at $\lambda = 370\, nm$.

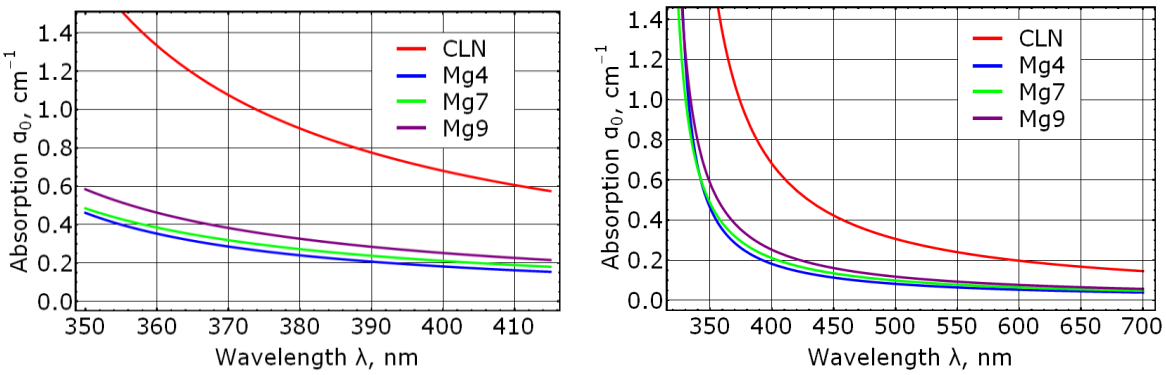

Fig. 6. Optical absorption vs. the incident light wavelength λ : within a wide spectrum (a) and in near-ultraviolet range (b) for various concentration of Mg. Solid lines are for infinitely small incident optical power density, i.e. for $\alpha_0(\lambda)$, while dotted lines are for the above-described combined spectral flux, i.e. at the saturation

Anyway, the plots presented in Fig. 6b can be interpreted as the presence of total optical losses $\alpha_T = \alpha_0 + \alpha_2 I(x)$ consisting of the basic absorption $\alpha_0(\lambda)$ together with an additional contribution $\alpha_2 I(x)$, where the dispersive factor $\alpha_2(\lambda)$ describes the nonlinear light-induced absorption. The last contribution depends on the external light flux $I(x)$, which is varied during its propagation along a crystal due to optical losses, while $I(x=0) = I_0$. In the case when I_0 can be considered as an infinitely small value, one yields the absence of the light induced absorption with linear losses $\alpha_T \approx \alpha_0$. By this it means that an effect of the self-action takes place, and in the supposition of exponential attenuation, one can write, for example,

$$I(x) \approx I_0 \exp\left[-(\alpha_0 + \alpha_2 \{ I_0 \exp\left[-(\alpha_0 + \alpha_2 I_0)x\right] \} x)\right] \qquad (16)$$

in the second approximation. As it follows from Eq.(16), the assumed difference of 10% does not look too dramatically from the viewpoint of losses within the doped $LiNbO_3$ crystal based AOF. Therefore, for the illustrative difference of 10% one can conclude that the doped $LiNbO_3$ crystal length in AOF can be estimated from the diagram presented in Fig. 7. Thus, for instance, the aforementioned 4% Mg doped $LiNbO_3$ crystal is able to provide the crystal length about $8\, cm$ at $\lambda = 370\, nm$ with the optical losses $\alpha_0(\lambda) \approx 0.28\, cm^{-1}$ as well as the length close to $13\, cm$ at $\lambda = 405\, nm$ with the optical losses $\alpha_0(\lambda) \approx 0.17\, cm^{-1}$, if the chosen optical transmittance ~ 10% is technically acceptable. For comparison, the plots related to the visible range at $\lambda = 532\, nm$ with $\alpha_0(\lambda) \approx 0.07\, cm^{-1}$ are shown as well.

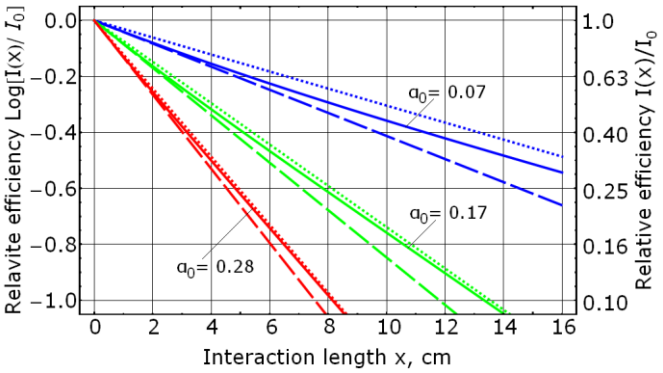

Fig. 7. Level of optical losses vs. 4%: $Mg-$ doped $LiNbO_3$ crystal length: the dotted straight lines are for the best case, i.e. for only the linear losses $\alpha_T \approx \alpha_0$, the dashed straight lines are for the worst case, i.e. for optical losses $\alpha_T = \alpha_0 + \alpha_2 I_0$, and the solid curves are for varying α_T in the second approximation, described by Eq.(16)

These plots demonstrate that one can observe some dynamics in varying losses. On the one hand, an ideal case corresponds to the absence of light-induced absorption when only the linear losses give their contribution and $\alpha_T \approx \alpha_0$ due to an infinitely small value of I_0, see the dotted straight lines in Fig. 7. On the other hand, the formal theoretical limit $\alpha_T = \alpha_0 + \alpha_2 I_0$ can be noted near the input facet of a crystal, see the dashed straight lines in Fig. 7. Physically, the initial maximal optical losses $\alpha_T = \alpha_0 + \alpha_2 I_0$ exhibit depletion of light-induced contribution together with reducing the light flux $I(x)$, so that optical losses will slowly approach to $\alpha_T \approx \alpha_0$, see the solid curves in Fig. 7 described by Eq.(16) in the second approximation.

4.1.3. Photorefraction

Photorefraction means changing the refractive indices caused by the rearrange of charges and holes in a material. Such changes, known also as "optical damage", are governed by the incident optical field, and they depend on the intensity of that field. There is a chance to use $LiNbO_3$ crystals, which is supported by the improved optical damaged resistance in Mg doped $LiNbO_3$ crystals [16,17] for the AOFs in near ultraviolet range [18]. Let us start from so-called uniform nonlinear photorefraction, when the effect of photorefraction does not exhibit any dependence on coordinates and time. Quantitatively, the uniform photorefraction in $LiNbO_3$ crystals under the action of an external optical beam with the particular light wavelength λ can be estimated as a variation of the birefringence $\delta|\Delta n|_\lambda$ using the scalar expression [20]

$$\delta|\Delta n|_\lambda \cong \frac{Rk\, I_{0,\lambda}\, \alpha_0(\lambda)}{\sigma_C} \ . \qquad (17)$$

Here, $|\Delta n|$ is the birefringence of a crystal, R is the generalized electro-optical coefficient, k is the Glass constant, $I_{0,\lambda}$ is the incident light intensity at the individual light wavelength λ, and $\sigma_C = \sigma_D + \sigma_P$ is the conductivity, in which σ_D is the dark conductivity and σ_P is the

photoconductivity. For the sake of simplicity, one can consider the factors R, k, and σ_C as the values independent of the optical wavelength in Eq.(17). One can see the directly proportional dependence between the light-induced birefringence change $\delta|\Delta n|_\lambda$ and the optical absorption factor $\alpha_0(\lambda)$ depending only on the optical wavelength remaining unaltered. After that, one can examine the data related to the optical absorption factor $\alpha_0(\lambda)$ and the light-induced birefringence change $\delta|\Delta n|_\lambda$ [21], which have been measured in the saturation regime and are valid, consequently, for long exposure times. These data had been obtained in the congruent $LiNbO_3$ crystal (CLN) and in the congruent $LiNbO_3$ crystal doped by 4 % of Mg (Mg4) to increase the resistance to photorefraction. With these results, it is possible to estimate the spectral dependence for the light-induced birefringence change $\delta|\Delta n|_\lambda$ in 4% Mg doped $LiNbO_3$ crystal.

Figure 8 illustrates the effect of photorefraction in $LiNbO_3$ crystals in the near ultraviolet range. One can see that the use of an adequate amount of Mg as a dopant improves the resistance to photorefraction in comparison with an undoped $LiNbO_3$ crystal. For optical wavelengths larger than $370\,nm$, the contribution of the photorefractive effect remains constant up to mid infrared wavelengths. As it is seen in Fig. 8, the photorefraction effect is reasonable for the congruent $LiNbO_3$ crystal (CLN) at the wavelengths longer than $340\,nm$. Nevertheless, this situation can be definitely improved with the use of the congruent 4% Mg doped $LiNbO_3$ (Mg4) crystal whose acceptable level of photorefraction is shifted down to about $320\,nm$.

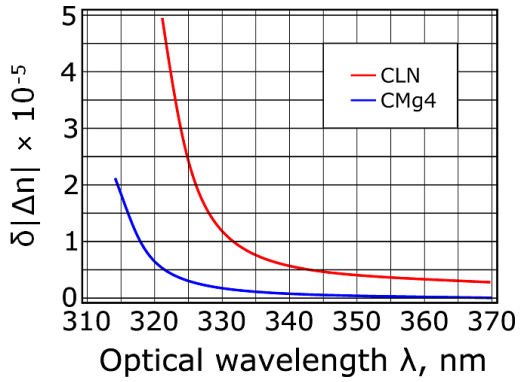

Fig. 8. Spectral dependencies for the light-induced birefringence change $\delta|\Delta n|_\lambda$: in the congruent $LiNbO_3$ crystal (red line) and in the congruent $Mg:LiNbO_3$ (blue line)

Then, as it had been described in section 3.1, the total dispersive optical losses are given by $\alpha_T = \alpha_0 + \alpha_2 I(x)$. Now, the product $\alpha_0(\lambda) I_{0,\lambda}$ in Eq.(17) has to be substituted by the other product $\alpha_T(\lambda)\, I_\lambda(x)$, which looks as

$$\alpha_T\, I(x) = I_0 \exp\left[-(\alpha_0 + \alpha_2\, I_0)\, x\right] \left(\alpha_0 + \alpha_2\, I_0 \exp\left\{-\left[\alpha_0 + \alpha_2\, I_0\right) x\right]\right\}\right) \qquad (18)$$

in a reasonable approximation. For infinitely thin samples $x \to 0$ or for infinitely small light flux intensity $I_0 \to 0$, Eq.(18) leads to

$$\text{a)}\ \alpha_T\, I(x) = I_0\,(\,\alpha_0 + \alpha_2\, I_0\,)\,, \qquad \text{b)}\ \alpha_T\, I(x) \approx \alpha_0\, I_0 \exp\,(-\alpha_0\, x)\,, \tag{19}$$

respectively. When $x \to 0$ and $I_0 \to 0$ together, Eqs.(19a) and (19b) give the same limit $\alpha_T\, I(x) \approx \alpha_0\, I_0$ as it was in Eq.(17). It is seen from Eq.(18) that even using that approximation, one arrives at nonlinear photorefraction, whose effect is decreasing with increasing the length of a crystal. Therefore, for really thick samples, about 10 cm and more, one has to apply exponential coordinate dependences, which involve remarkably faster attenuation into consideration. This reduction in the photorefraction effect leads, in fact, to additional variations of the birefringence along a crystal, i.e. to another kind of non-uniformity for the birefringence that affects performances of the AOF. At the same time, one can keep a minimum of terms that includes the initial light intensity I_0, which can be small in practice. In doing so, Eq.(18) can be expanded into a series as

$$\alpha_T\, I(x) \approx I_0 \exp\,(-\alpha_0\, x)\,\{\alpha_0 + \alpha_2\, I_0\,[\exp\,(-\alpha_0 x) - \alpha_0 x]\,\} \tag{20}$$

in the second approximation with respect to the intensity I_0, which gives both the Eqs.(19) in those limits.

At this step, rather well grounded experimentally supposition can be made. Namely, variations of the birefringence $\delta\,|\Delta n|_\lambda$ are additive in behavior when, for example, a few optical beams with various light wavelengths will be directed on a crystal. By this it means that, in the case of a black body radiation with the incident spectral flux density $F(\lambda)$, the combined effect of photorefraction within all the spectral range $\Delta\lambda$ under action of the total flux I_0 can be estimated from Eqs.(17) and (9) as

$$\text{a)}\ \delta\,|\Delta n| \cong \frac{Rk}{\sigma_c} \int_{\Delta\lambda} \Bigg\{\ \alpha_0(\lambda_0) \exp\,[-\alpha_0(\lambda_0)\, x] + \Bigg[\exp\,[-\alpha_0(\lambda_0)\, x]\,\{\exp\,[-\alpha_0(\lambda_0) x] - \alpha_0(\lambda_0) x\} \int_{\Delta\lambda} \alpha_2(\lambda_0, \lambda_1)\ F(\lambda_1)\, d\,\lambda_1\Bigg]\Bigg\} F(\lambda_0)\, d\,\lambda_0,$$

$$\text{b)}\ I_0 = \int_{\Delta\lambda} F(\lambda)\, d\,\lambda\,. \tag{21}$$

Because of the data from Fig. 8, the lower bound of integration in Eq.(21) must be taken close to $320\,nm$ or higher to reduce the potential influence of photorefraction. Practically, the expected range of observations is narrow enough, so that one can consider the incident spectral flux density $F(\lambda)$ as almost constant of λ and take $F(\lambda)$ out of the corresponding integrals in Eq.(21). In doing so, one can obtain a quadratic algebraic equation relative to $F(\lambda)$ from Eq.(21a) and find

$$\text{a)}\ \frac{\sigma_C\ \delta\,|\Delta n|}{R\ k_0} \approx A_0(x) F + A_1(x) F^2\,, \qquad \text{b)}\ A_0(x) = \int_{\Delta\lambda} \alpha_0(\lambda_0) \exp\,[-\alpha_0(\lambda_0)\, x]\, d\,\lambda_0\,,$$

$$\text{c)}\ A_1(x) = \int_{\Delta\lambda} \Bigg[\exp\,[-\alpha_0(\lambda_0)\, x]\,\{\exp\,[-\alpha_0(\lambda_0) x] - \alpha_0(\lambda_0) x\} \int_{\Delta\lambda} \alpha_2(\lambda_0, \lambda_1)\, d\,\lambda_1\Bigg]\, d\,\lambda_0\,. \tag{22}$$

$$F \cong \frac{1}{2A_1^2(x)}\left[-A_0(x)+\left(A_0^2(x)+4A_1(x)\cdot\frac{\sigma_C\,\delta\,|\Delta n|}{R\,k_0}\right)^{1/2}\right]. \qquad (23)$$

Now, one has to establish a proper criterion for estimating an acceptable level of photorefraction, which still does not affect performances of the AOF, in particular, its spectral resolution. For this purpose, we suggest to use the criterion that had been exploited before for the optical non-uniformity ΔB of birefringence in a crystal during our analysis of optical imperfectness along a crystal, see Eq.(14). In our case, the same birefringence $|\Delta n| \approx 0.1$ is for both the congruent $LiNbO_3$ crystal (CLN) and the 4% Mg doped $LiNbO_3$ (Mg4) crystal.

By this it means that rather acceptable level of photorefraction, considering a homogeneous change in the birefringence over all the spectral range, can be estimated by the value $\delta\,|\Delta n| \le 10^{-6}$. Then, using Eq.(23), one can estimate the maximum incident spectral flux density measured in $W/(mm^2 Å)$, under action of which the effect of photorefraction on optical properties of $LiNbO_3$ crystals is small enough to be neglected, i.e. for which the photorefraction will be acceptable due to $\delta\,|\Delta n| < 10^{-6}$.

If the product $A_1(x=0)\,F$ in Eq.(22a) can be considered as a small value in comparison with $A_0(x=0)$, the first approximation can be used for estimating the maximum flux density $F(\lambda)$. Consequently, one can obtain

$$F \cong \frac{\sigma_C\,\delta\,|\Delta n|}{R k_0\,A_0(x=0)}\ . \qquad (24)$$

Using the above-noted threshold for acceptable photorefraction, one can estimate the limits for the spectral flux density by $F_{\max} \le 43\,\mu W/(mm^2 Å)$ in the $LiNbO_3$ and $F_{\max} \le 355\,\mu W/(mm^2 Å)$ for the 4% Mg doped $LiNbO_3$ within the spectral range $\Delta\lambda$ from $320\,nm$ to $700\,nm$. Thus we can be sure that it will be possible to neglect the photorefractive effect in the potential AOF.

5. SCHEME FOR THE EXPERIMENTS WITH A COLLINEAR ACOUSTO-OPTICAL CELLS

To realize experimentally the process of collinear interaction we have used the scheme shown in Fig.9. It consists of a continuous-wave laser, an acousto-optical cell with a pair of the Glan-Taylor crystalline polarizers (with the extinction ratio 10^5 each) whose combined layout is presented in details in Fig.10, a silicon photo-detector, and a set of electronic equipment for both generating and registering the corresponding electric ultra-high-frequency (UHF) radio-wave signals. Initially, the tunable UHF-signal is applied to the electronic input port of the collinear acousto-optical cell through a wide-band UHF-amplifier HD18858 ($10-1000\,MHz,\ 8\,W$), see Figs.9 and 10, and to the input of an oscilloscope (or computer) as the etalon signal, see Fig.9.

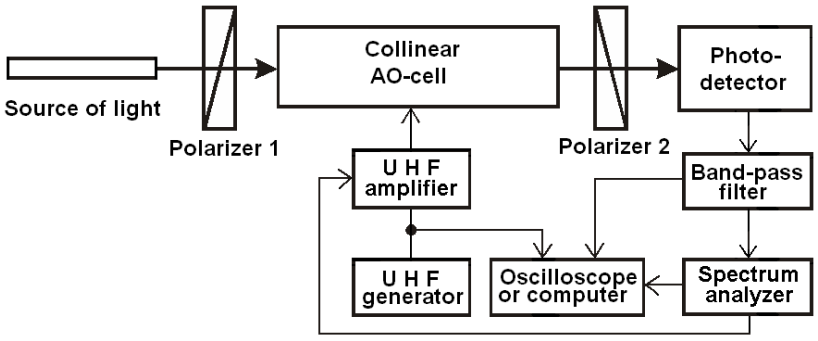

Fig.9. Schematic arrangement of the experimental set-up

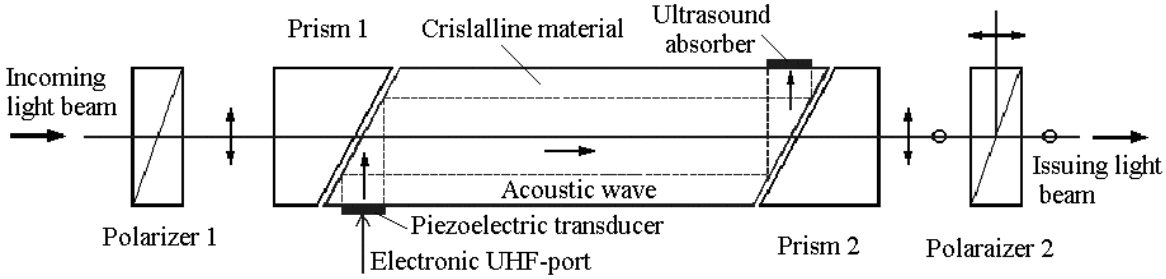

Fig.10. Scheme of the co-propagating collinear acousto-optical cell providing the traveling-wave regime of interaction between the pumping light beam and the continuous-wave acoustic beam experiencing moderate linear losses.

6 EXPERIMENTS WITH COLLINEAR ACOUSTO-OPTICAL FILTERS

6.1 Calcium molybdate cell

A two-mode co-propagating collinear $CaMoO_4$ crystalline cell was characterized by a crystal length $L = 4.4\,cm$ along the $[100]$-axis, an acoustic velocity $V = 2.95 \cdot 10^5\,cm/s$ for the shear elastic mode whose displacement vector is oriented along the $[001]$-axis. The continuous-wave beam at a dark-red light wavelength of $\lambda = 671\,nm$ (the output optical power $\sim 40\,mW$) had been chosen, first, to minimize the controlling acoustic wave frequency down to about $35\,MHz$ in a view of realizing as close as possible "almost lossless" regime for the propagation of acoustic beam through the $CaMoO_4$ crystalline cell and, second, to keeping just the visible range of operation with light beams simplifying the experimental conditions of observations. The continuous-wave beams (the output optical power $\sim 30-40\,mW$) from a red light wavelength of $\lambda = 633\,nm$ to dark-blue with $\lambda = 444\,nm$ had been used as an optical pump during the experiments providing the traveling-wave regime of interaction between the pumping light beam and the acoustic wave. It had been done, first, to keep just the visible range of operation with light beams simplifying the experimental conditions of observations. Then, the visible range of light overlaps rather wide range of acoustic frequencies ($35-95\,MHz$) and makes accessible varying the acoustic losses as much as possible (about 5 times) due to a square-law dependence of the attenuation on the frequency. Turning back to the scheme, the first polarizer was precisely aligned in correspondence with the optical axes of a crystal in a cell. As the optical pump and the continuous-wave acoustic wave were interacted, already two orthogonally polarized light beams, incident and signal ones, passed through a cell. The second polarizer gave us an opportunity to be aligned in correspondence with the polarization of the signal beam and to extract the output optical signal, see Fig.10. Then, one can restrict oneself by a maximal level $P \le 0.5\,W/mm^2$ of acoustic power density, which is conditioned by the absolute acoustic power magnitude of about $2\,W$ and the acoustic beam cross section of about $4\,mm^2$ in the chosen collinear cell. Consequently, one can calculate that $\sigma \le 2\,cm^{-1}$. These estimations demonstrate that the above-noted limitations on both the needed acoustic power densities and the magnitudes of the parameter σ, related to the firsts extrema, lie in the frames of acceptable values.

6.1.1. Lossless case

The nonlinear dynamics of varying the transition functions of the optical filter under consideration has been sequentially followed during our experiments as the acoustic power density of finite amplitude grows. A few examples of the corresponding digitized oscilloscope traces are shown in Fig.11

Now, let us discuss this set of oscilloscope traces for the scattered light component intensity $|C_1|^2$ detected during the experiments with the collinear $CaMoO_4$ crystalline cell ignoring the acoustical losses due to low acoustic frequency and estimated at the level 0.405 conditioned by the Rayleigh criterion. All these traces can be easily interpreted in terms of the above-developed theory taking into account that. The first trace in Fig.11a reflects the filter transition function inherent in almost the regime with infinitely small amplitude of the controlling acoustic signal due to the

dimensionless value $\sigma L = 0.21$ is very close to zero. This value (which is non-zero, in fact) had been taken as an example to show rather adequately conventional representation for the transition function width or, what is the same, the filter frequency resolution, being close to $\delta f \approx V / L \approx 68.44\, kHz$, as well as to have a chance for identifying the output response whose relative intensity is small enough, i.e. even less then $5\,\%$. The second and third traces, peculiar to $\sigma L \approx 1.0$ and $\sigma L \approx \pi / 2$ are presented in Figs.11b and 11c, respectively. From a viewpoint of widely used acousto-optic approach, they can be considered as a natural testimony of growing the relative intensity of the output optical signal up to 0.715 and ~ 1.0 under action of the increasing acoustic power density.

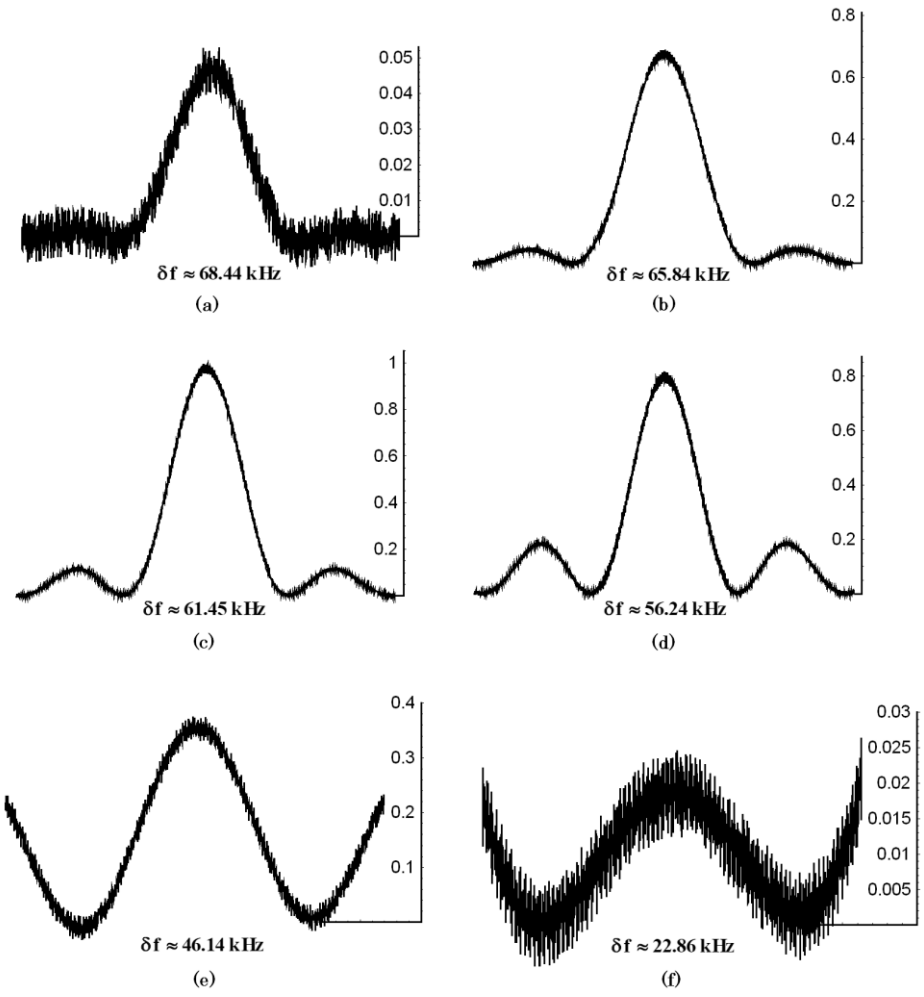

Fig. 11. The digitized oscilloscope traces for the scattered light intensity $|C_1|^2$ observed at the output of the collinear $CaMoO_4$ cell at the carrier acoustic frequency of $\sim 37.3\, MHz$ and estimated at the level 0.405. Reshaping the transmission function is followed at the same optical pump in variable scales:

(a) $\sigma L = 0.21$, $P \approx 0.00104\,[W/mm^2]$; (b) $\sigma L \approx 1.0$, $P \approx 0.0236\,[W/mm^2]$;

(c) $\sigma L \approx \pi / 2$, $P \approx 0.0582\,[W/mm^2]$; (d) $\sigma L \approx 2.0$, $P \approx 0.0944\,[W/mm^2]$;

(e) $\sigma L \approx 2.5$, $P \approx 0.148\,[W/mm^2]$, and (f) $\sigma L \approx 3.0$, $P \approx 0.223\,[W/mm^2]$.

They both exhibit the optical resolution of more or less the same order, which varies slightly from the above-mentioned $68.44\,kHz$ to $\delta f \approx 65.84\,kHz$ and $\delta f \approx 61.45\,kHz$, respectively. Such a conclusion looks rather plausible within quasi-linear approximation for the transition function as well as in the course of possible measurements in the frequency domain with not enough accuracy. Nevertheless, further increase of the acoustic power density, depicted by the traces with $\sigma L \approx 2.0$ and $\sigma L \approx 2.5$ in Figs.11d and 11e, is able to demonstrate step by step that the existing specific acousto-optical nonlinearity leads to squeezing the transition function or to improving the frequency resolution to $\delta f \approx 56.24\,kHz$ and $\delta f \approx 46.14\,kHz$, respectively. This process is accompanied by decreasing the relative intensity of the output optical beam down to about 0.82 and 0.35 in the so chosen points. Finally, the last trace, see Fig.11f, illustrates obviously nonlinear process of squeezing the transition function or improving the frequency resolution in the vicinity of the first point $\sigma L = \pi$ of a collapse. Namely the value $\sigma L \approx 3.0$ has been taken to have an opportunity for revealing the transition function characterized by $\delta f \approx 22.86\,kHz$ whose relative intensity becomes already dramatically small and does not exceed $2\,\%$.

6.1.2. Lossy case

A triplet of experiments had been carried out. At first, the scattered light intensity $|C_1|^2$ as the function of the acoustic power density P with the fixed length of interaction $L = 4.4\,cm$ had been registered under condition of $P \le 0.5\,W/mm^2$ (i.e. $\sigma \le 2\,cm^{-1}$). To identify better the expected influence of moderate linear losses on the transmission functions of that cell the maximal acceptable acoustic frequency $f_{\max} = 94.34\,MHz$, accompanied by $\lambda = 444\,nm$, had been chosen to provide the highest possible for this cell acoustic attenuation $\alpha = 0.1152 \cdot \Gamma\, f_{\max}^2 \approx 0.0615\,cm^{-1}$. For the comparison, the similar plot for $\alpha = 0.0261\,cm^{-1}$ related to $f = 61.24\,MHz$ and $\lambda = 532\,nm$ has been chosen. The corresponding experimental plots are depicted in Fig.12. One can see that a few extrema, namely, two maxima and one zero had been achieved at each optical wavelength and registered during the measurements carried out. The presented here trace for $\lambda = 532\,nm$ can be compared with the theoretical plot.

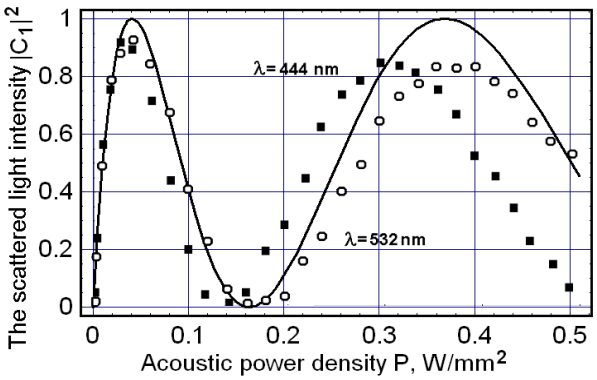

Fig.12. The scattered light intensity $|C_1|^2$ versus the acoustic power density P with $\alpha = 0.0261\,cm^{-1}$ (solid line is for theory and circles are for experiment at $f = 61.24\,MHz$, $\lambda = 532\,nm$) and $\alpha = 0.0615\,cm^{-1}$ (squares are for experiment at $f_{\max} = 94.34\,MHz$, $\lambda = 444\,nm$) in the $CaMoO_4$-cell.

Merely the presence of moderate linear acoustic losses is able to affect the width of the transmission function. Reshaping the transmission function has been followed with approximately one and the same input optical pump at various light wavelengths and at very close to one another values of the product σL, which all can be characterized as "rather small" in a view of realizing a limit to infinitely small input acoustic signals. To keep a balance between as low as acceptable level of the acoustic power in that limit, on the one hand side, and to have an option for reliable measurements of the transmission function width, on the other hand side, the product $\sigma L \approx 0.2$ had been chosen experimentally. In fact, fixing this product leads, nevertheless, to $\sigma = 0.04545\, cm^{-1}$ and remarkably different levels of the needed acoustic power densities $P[W/cm^2] \approx 0.27 \cdot (\lambda[\mu m])^2$ for its realization.

A few examples of the corresponding digitized oscilloscope traces, estimated at the level of 0.405 conditioned by the Rayleigh criterion, are shown in Fig.13. These traces for the scattered light intensity $|C_1|^2$ had been observed at the output of the above-described collinear $CaMoO_4$ cell at various carrier acoustic frequencies, which provide various magnitudes of the linear acoustic losses depending quadratically on those frequencies.

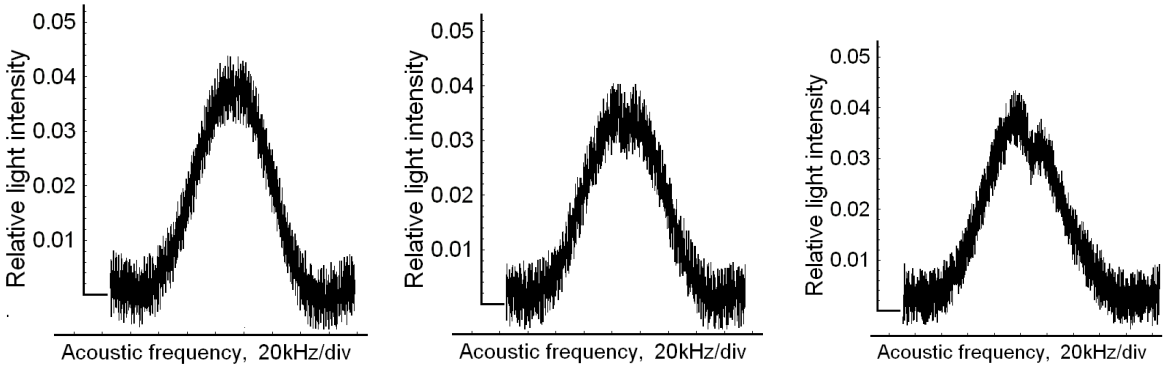

(a) $\delta f \approx 69.45\, kHz$ (b) $\delta f \approx 71.03\, kHz$ (c) $\delta f \approx 75.74\, kHz$

Fig.13. The digitized oscilloscope traces for the scattered light intensity $|C_1|^2$ observed at the output of the collinear $CaMoO_4$ cell for various acoustic losses and acoustic frequencies. Their widths have been measured at the level 0.405 with $\sigma L \approx 0.2$, so that: (a) $f_A = 43.47\, MHz$, $(\alpha L)_A \approx 0.0575$; (b) $f_B = 61.24\, MHz$, $(\alpha L)_B \approx 0.114$; and (c) $f_C = 94.34\, MHz$, $(\alpha L)_C \approx 0.271$.

Finally, the effect of non-linear narrowing had been observed via measuring the widths peculiar to profiles of the scattered light intensity $|C_1|^2$ as a function of the applied acoustic power density explained in terms of the dimensionless product σL. For this purpose, we had taken the regime of scattering the green light with $\lambda = 532\, nm$ connected with the acoustic wave frequency $f_0 = 61.24\, MHz$, which provides sufficiently tangible total acoustic attenuation $\alpha L \approx 0.114$ all over the cell aperture. At first, both the 2D-theoretical plots with the product $\alpha L \approx \{0, 0.0575, 0.114, 0.271\}$ and the observed experimental data as points are combined in Fig.14.

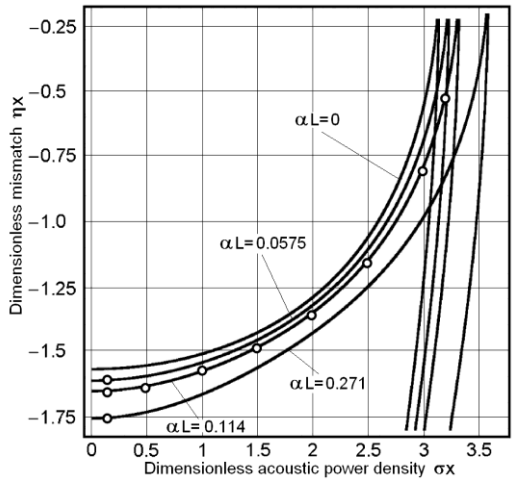

Fig.14. Combined diagram reflecting both the 2D-theoretical plots with the product $\alpha L \approx \{0, 0.0575, 0.114, 0.271\}$ and all the above-noted experimental points. The lossless case is $\alpha L = 0$.

Then, the oscilloscope traces for the scattered light component intensity $|C_1|^2$ detected during the experiments with the collinear $CaMoO_4$ crystalline cell and estimated at the level 0.405 conditioned by the Rayleigh criterion, see Fig. 15. All these traces can be interpreted in terms of the above-developed theory.

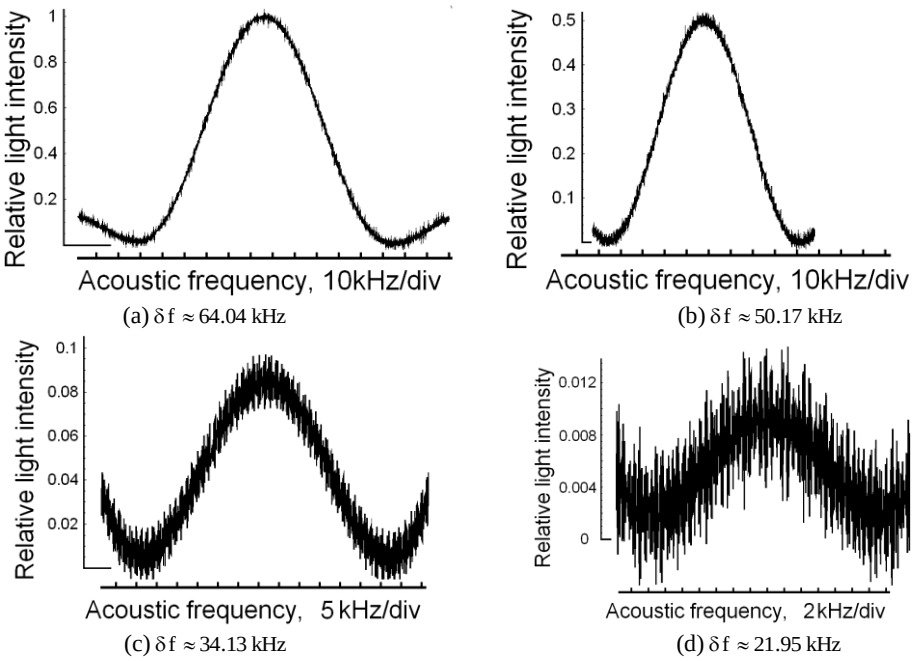

Fig.15. The digitized oscilloscope traces for the scattered light intensity $|C_1|^2$ for the green light with $\lambda = 532\ nm$ observed at the output of the collinear $CaMoO_4$ cell near the central carrier acoustic frequency $f_0 = 61.24\ MHz$ and estimated at the level 0.405. Reshaping the transmission function is followed at the same optical pump in variable scales: (a) $\sigma L \approx \pi/2$, $P \approx 0.0365\ [W/mm^2]$; (b) $\sigma L \approx 2.5$, $P \approx 0.0925\ [W/mm^2]$, (c) $\sigma L \approx 3.0$, $P \approx 0.133\ [W/mm^2]$, and (d) $\sigma L \approx 3.2$, $P \approx 0.152\ [W/mm^2]$.

6.2. *Lithium niobate cell*

A two-mode co-propagating $LiNbO_3$-crystalline collinear AOC was characterized by the interaction length $L \approx 6.3\,cm$ along the $[010]$-axis and the acoustic velocity $V = 3.96 \cdot 10^5\ cm/s$ for the pure slow shear elastic mode whose displacement vector was oriented along the $[100]$-axis, see Fig.16.

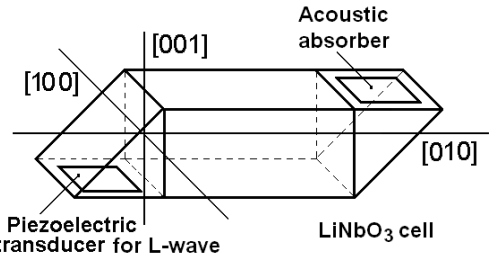

Fig.16. Arrangement of the a two-mode co-propagating collinear $LiNbO_3$ AOC

The continuous-wave (CW) light beams from the solid-state lasers (CrystaLaser; the output optical power $\sim 30\,mW$; $\lambda = 405\,nm$ and $440\,nm$; transverse mode TEM_{00}; single longitudinal mode, providing narrow enough for our goals optical spectral lines) had been used as a CW optical pump during the experiments with the traveling-wave regime of interaction between the pumping light beam and the acoustic wave. It had been done at $\lambda = 405\,nm$ and $440\,nm$ to keep just the visible range of operation (and not to go in a near ultraviolet range) for simplifying experimental observations. Turning back to the scheme, the first polarizer was precisely aligned in correspondence with the optical axes of a crystal in a cell and along the polarization vector of the incident beam. As the CW optical pump and the CW acoustic wave were interacted, already two orthogonally polarized light beams, initial incident and appeared signal ones, passed through a cell. The second polarizer gave us an opportunity to be aligned along the polarization vector of the signal beam and to extract the output optical signal, see Fig.12. Then, one had to restrict oneself by the maximum level $P \le 0.1\,W/mm^2$ of acoustic power density, which is conditioned by the absolute acoustic power magnitude of about $2\,W$ and the acoustic beam cross section area of about $4\,mm^2$ in the chosen collinear cell. Not all the functional connections shown in Fig.12 had been exploited at the same time. At least three regimes can be separated. One of them was related to measuring the light intensity dependences at the fixed acoustic carrier frequency. Two others were connected with estimating the frequency dependencies at stepwise variations of the applied acoustic power. They both include exploitation of the sweep-generator from spectrum analyzer and provide operating with the band-pass filter (bandwidth $\sim 5\,kHz$) and oscilloscope as well as with the spectrum analyzer (bandwidth $\le 10\,Hz$), in particular, for calibrations and accurate measurements of frequency.

Using the experimental data, one can create the combined diagrams, which include theoretical plots for the spectral resolution $\delta\lambda$ and the relative scattered light intensity I versus the acoustic power density P of the above-noted slow shear acoustic mode at $\lambda = 405nm$ with $f = 1.04\,GHz$, $\alpha = 0.0991\,cm^{-1}$, $\alpha_0 \approx 0.17\ cm^{-1}$ and at $\lambda = 440\,nm$ with $f = 0.896\,GHz$, $\alpha = 0.0740\ cm^{-1}$, $\alpha_0 \approx 0.12\ cm^{-1}$, see Fig.17.

The congruent $LiNbO_3$ (CLN) exhibits a higher optical absorption coefficient as compared with 4% Mg doped $LiNbO_3$. Theoretically speaking, this fact decreases the transparency of the congruent $LiNbO_3$ crystal and therefore, the efficiency is reduced considerably. For example, the peak efficiency of about 30% for Mg4–crystal at $\lambda = 405\,nm$ falls down to the peak efficiency of about 5% for CLN–crystal at the same wavelength. Nevertheless, the expected spectral resolution is not affected dramatically. Following the previous example, the spectral resolution for the peak efficiency is about 0.25 Å for both the cases under the same acoustic power density.

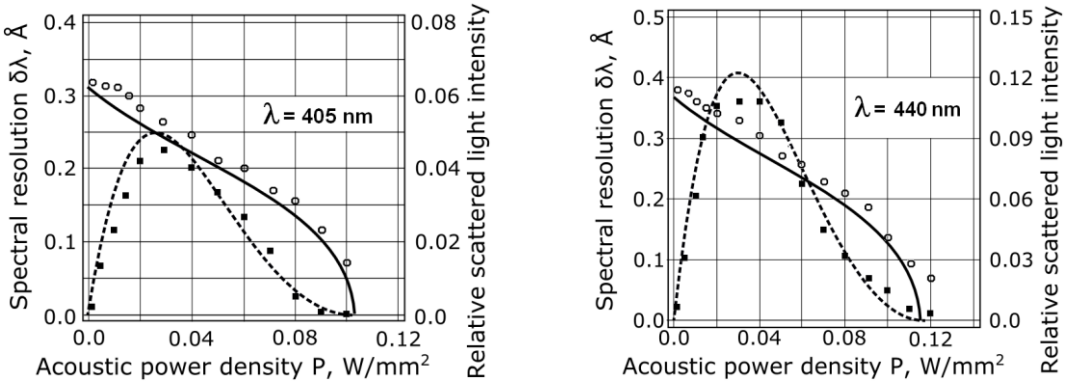

a. 405 nm (63 mm) **b. 440 nm (63 mm)**

Fig. 17. Combined plots of the spectral resolution $\delta\lambda$ and the relative scattered light intensity vs. the acoustic power density P for the pure slow shear elastic mode passing along the $[010]$-axis in the congruent $LiNbO_3$-crystal: (a) at $\lambda = 405\,nm$, $f = 1.04\,GHz$, $\alpha = 0.0991\,cm^{-1}$, $\alpha_0 \approx 0.17\,cm^{-1}$ and (b) at $\lambda = 440\,nm$, $f = 0.896\,GHz$, $\alpha = 0.0740\,cm^{-1}$, $\alpha_0 \approx 0.12\,cm^{-1}$. Here, the solid lines (theory) and circles (experiment) are for the spectral resolution $\delta\lambda$, while the dotted lines (theory) and squares (experiment) are for the relative efficiency of the light scattering.

In Fig.17, the experimental data provide a spectral resolution δλ, which is just marginally larger than the theoretical prediction, at both the wavelengths and along all the range of acoustic power density. In particular at λ = 405 nm, the average exceeding is about 0.019 Å, while at 440 nm the experimental value of δλ is in average about 0.022 Å larger than the theory predicts (excluding the point at P = 0.12 W/mm^2). As far as the relative scattered light intensity, i.e. the efficiency of operation is concerned; we observe relatively good agreement of the experimental data with the theoretical curves all over the probed acoustic power density P interval. However, the experimental maxima are lower (of about 0.0041 at 405 nm and about 0.0065 at 440 nm), although experimentally observed locations of efficiency peaks on the P-axes coincide with the theoretical predictions. The non-coincidences between theoretical and experimental peaks in magnitudes of the relative scattered light intensities are about 8% and 12% at 405 nm and 440 nm, respectively.

Generally, the differences between theoretical performances and the experimentally obtained data shown in Fig.17 indicate that evidently not all the phenomena (maybe even some of the omitted ones) associated with the effect under consideration had been taken into account, so that our theoretical model could be potentially improved. The last one is true especially for areas of relatively higher acoustic power density. Nevertheless, the smallness of those differences confirms

substantially the opportunity to make the above-chosen approximations, i.e. omitting some terms in Eq.(14) from our model.

The oscilloscope traces of the scattered light intensity $|C_1|^2$ have been detected during the experiments with collinear congruent $LiNbO_3$ – crystalline AOC and measured at the level 0.405 in agreement with the Rayleigh criterion, see Fig.18.

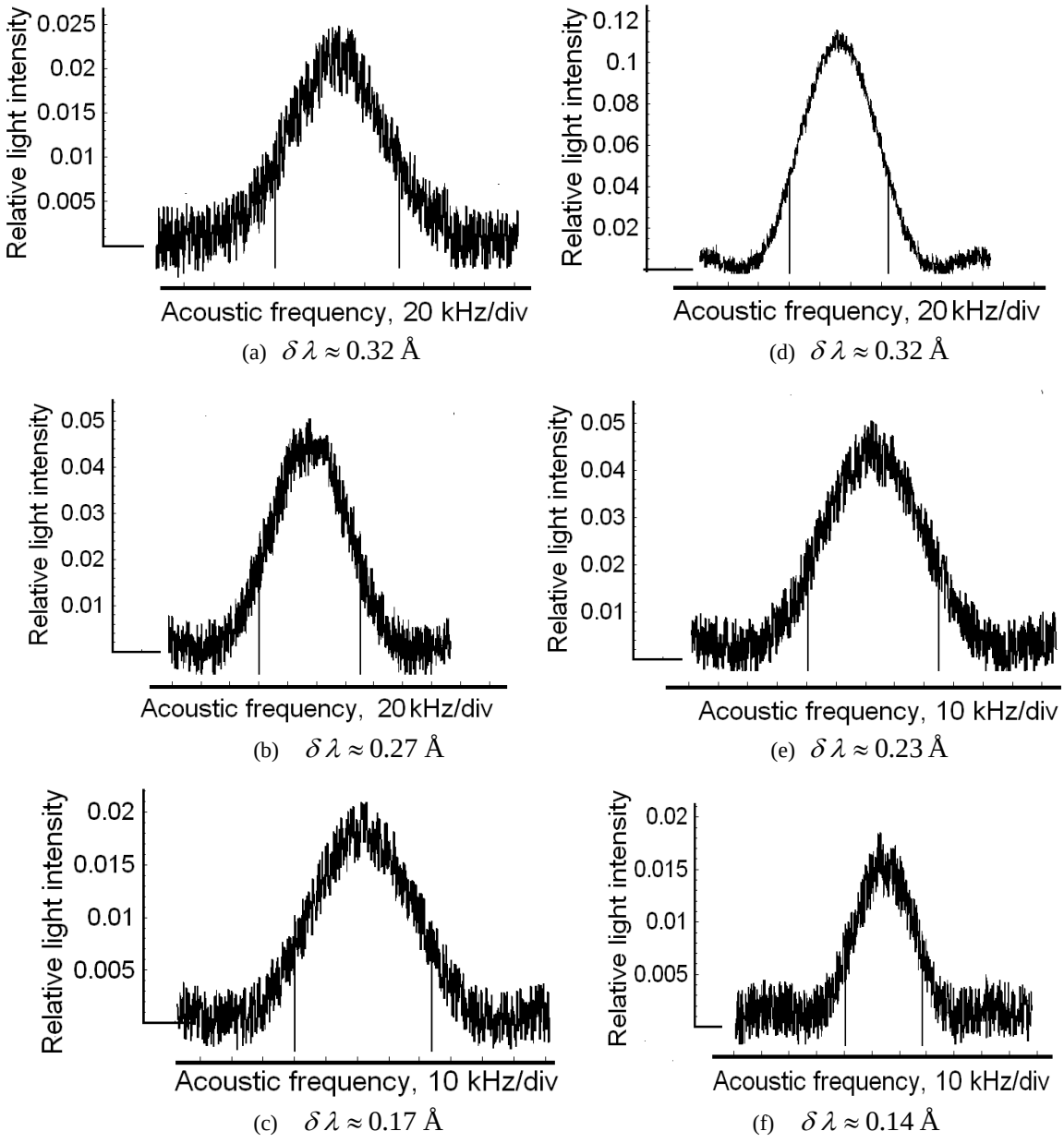

Fig. 18. The digitized oscilloscope traces for the scattered light intensity $|C_1|^2$ observed at the output of the collinear congruent $LiNbO_3$ – AOC with $L \approx 6.3\ cm$ for various acoustic power densities.
(a, b, c) for 405 nm, (d, e, f) for 440 nm, See Table 1 and 2 respectively, for more details.

All these traces can be interpreted in terms of the developed theory. Narrowing the transmission functions is accompanied by decreasing the relative intensity of the output light beam. Varying the transmission functions widths have been followed providing the same input optical pump and light wavelength at the acoustic power density, which all can be characterized as "rather small" in a view of implementing a limit of infinitely small input acoustic signals. To keep a balance between as low as acceptable level of the acoustic power in this limit, on the one hand, and to have an option for reliable measurements of the transmission function width, on the other hand, the acoustic power density $P \le 0.1 W/mm^2$ with $\sigma \le 2\, cm^{-1}$ had been chosen experimentally to obtain the relative efficiency about 12.5%.

Table 1. Values for the width and normalized intensities of the transmission functions measured at $\lambda = 405\, nm$ and $f \approx 1.04\, GHz$ (see the left column traces in Fig. 18)

Power, W/mm^2	σ, cm^{-1}	δλ, Å	δf, kHz	I_1
0.01	0.635	0.32	82.24	0.023
0.03	1.10	0.27	69.39	0.045
0.07	1.68	0.17	43.69	0.018

Table 2. Values for the width and normalized intensities of the transmission functions measured at $\lambda = 440\, nm$ and $f = 0.896\, GHz$ (see the right column traces in Fig 18)

Power, W/mm^2	σ, cm^{-1}	δλ, Å	δf, kHz	I_1
0.03	1.013	0.32	65.15	0.11
0.07	1.547	0.23	46.83	0.045
0.10	1.849	0.14	28.51	0.015

Results of our experiments illustrate nonlinear narrowing of the transmission function within propagation of the pure slow shear elastic wave with moderate acoustic losses through the collinear lithium niobate crystalline AOC that exhibits the light induced optical losses with an effect of the self-action and photorefraction for the incident light beam at $\lambda = 405\, nm$ and $440\, nm$. The nonlinear dynamics of varying the transmission function within collinear acousto-optical interaction is caused by the elastic waves of finite amplitude. This nonlinear effect gives us a chance for improving the spectral resolution peculiar to the congruent $LiNbO_3$-crystalline AOF, which exploits the slow shear elastic mode propagating along the $[010]$-axis. In fact, this regime realizes an opportunity to exchange a portion of the transmission efficiency inherent in the AOF for an improvement in its operation accuracy.

7. CONCLUSION

Thus, one can conclude that we have revealed nonlinear narrowing of the transmission function inherent in collinear acousto-optical interaction occurred by the acoustic waves in a medium with moderate losses. This nonlinear effect can be interpreted also as improving the spectral and frequency resolution peculiar to the equivalent collinear acousto-optical filter operated by the controlling acoustic waves of finite amplitude. In fact, we have found an opportunity to exchange a portion of transmittance for a portion of accuracy. Sometimes, for instance in astrophysical observations, it could be useful practically when extremely bright object is under optical spectrum analysis. Rather adequate theory of this effect has been developed analytically and illustrated via the corresponding computer simulations. In particular, a periodicity for the nonlinear narrowing of the transmission function, which includes a set of points for its collapses originating periodically, has been found and estimated. It has been shown that the first period of similar collapsing exhibits the best relation between the width and magnitude of the narrowed transmission function from the viewpoint of practical application. Then, the needed estimations have been performed for collinear interaction in the visible range in a $CaMoO_4$ and a $LiNbO_3$ crystals.

The transmission efficiency steeply increases with growing the light wavelength and with decreasing the length of similar AOF. Nevertheless, the efficiency of that AOF still remains higher than 30% in the near ultraviolet, if the spectral resolution is limited by $\delta\lambda = 0.28–0.29$ Å. However, we have demonstrated the possibility to reach the resolution as high as $\delta\lambda = 0.12–0.15$ Å ($R > 24600$), preserving at the same time an efficiency higher than 10% over all the spectral interval that we considered.

We have analyzed in their combined totality all the possible factors determining the efficiency of operation and spectral resolution. As a result, we have obtained the highest available spectral resolution for any collinear AOF to our knowledge. Then, we have also explored the opportunity to trade an amount of AOF's efficiency for an improvement in its spectrum resolution.

8. ACKNOWLEDGMENTS

This work had been financially supported by the CONACyT, Mexico (projects # 61237 and # 15149).

9. REFERENCES

1. R.W. Dixon, "Acoustic diffraction of light in anisotropic media", IEEE J. of Quantum Electronics. Vol.**QE-3**, no.2, 85-93 (1967).
2. S.E. Harris, R.W. Wallace, "Acousto-optic tunable filter", J. Opt. Soc. Am. Vol.59, no.6, 744-747 (1969).
3. S.E. Harris, S.T.K. Nich, R.S. Fiegelson, "$CaMoO_4$ electronically tunable optical filter", Appl. Phys. Lett. Vol.**17**, no.5, 223-225 (1970).
4. I.C. Chang, "Tunable acousto-optic filter utilizing acoustic beam walk-off in crystal quartz", Appl. Phys. Lett. Vol.**25**, no.9, 323-324 (1974).
5. J.A. Kusters, D.A. Wilson, D.L. Hammond, "Optimum crystal orientation for acoustically tuned optical filters", J. Opt. Soc. Am. Vol.**64**, no.4, 434-440 (1974).
6. E.T. Aksenov, N.A. Esepkina, A.S. Shcherbakov, "Acousto-optical filter with a $LiNbO_3$-crystal" Tech. Phys. Lett, Vol.**2**, no.3, 83-84 (1976).
7. J.D. Fichter, M. Gottlieb, J.J. Conroy. Appl. Phys. Lett. Vol.**34**, no.1, 1-3 (1979).

8. V.N. Parygin, AV. Vershubskii, K.A.Kholostov. “Control of the characteristics of a calcium molybdate collinear acousto-optic filter,” Technical Physics, Vol.44, no.12, 1467-1471 (1999).
9. V.I. Balakshy, V.N. Parygin, L.I. Chrkov. Physical Principles of Acousto-Optics, Radio I Svyaz, Moscow, 1985.
10. A. Korpel. Acousto-Optics, 2-nd Ed., Marcel Dekker, New-York, 1997.
11. F.T.S. Yu. Introduction to Information Optics, Academic Press, San Diego, 2001.
12. A. Mahieux, V. Wilquet, R. Drummond, et al. “A new method for determining the transfer function of an Acousto optical tunable filter,” Optics Express, Vol. **17**, Issue 3, pp. 2005-2014 (2009).
13. A.S. Shcherbakov, A. Aguirre Lopez, “Shaping the optical components of solitary three-wave weakly coupled states in a two-mode waveguide,” Optics Express. Vol.**11**, no.14, 1643-1649 (2003).
14. G. D. Boyd, W. L. Bond, and H. L. Carter, “Refractive Index as a Function of Temperature in $LiNbO_3$,” Journal of Applied Physics, **38**, 1941-1943 (1967).
15. A. Di Maio et al., “Spectral characterization of integrated acousto-optic tunable filters by means of laser frequency modulation spectroscopy,” Applied Optics **45** No. 36, 9176-9181 (2006).
16. D. A. Bryan, R. Gerson, and H. E. Tomaschke, “Increased optical damage resistance in lithium niobate,” Applied Physics Letters 44 847 – 849 (1984).
17. Sweeney K L et al., “Point defects in Mg-doped lithium niobate,” Journal of Applied Physics 57 1036 – 1044 (1985).
18. Minemoto H, Nishiyama T and Shibuya K. U. S. Patent No. 6,903,862 B2 (2005).
19. Waasem N et al., “Green-induced blue absorption in MgO-doped lithium niobate crystals,” Optics Letters 38 No. 16 2953-2956 (2013).
20. Volk T, Rubinina N and Wöhlecke M., “Optical-damage-resistant impurities in lithium niobate,” J. Opt. Soc. Am. B 11 No. 9 1681-1687 (1994).
21. Xin F et al., “Ultraviolet photorefraction at 325 nm in doped lithium niobate crystals,” Journal of Applied Physics 107 033113 (2010).